

Optimal diffusion of chiral active particles with strategic reorientations

Kristian Stølevik Olsen¹* and Hartmut Löwen²

Institut für Theoretische Physik II - Weiche Materie, Heinrich-Heine-Universität Düsseldorf, D-40225 Düsseldorf, Germany



(Received 26 June 2024; accepted 5 November 2024; published 17 December 2024)

We investigate the competing effects of the simultaneous presence of chirality and generalized tumbles in the dynamics of an active Brownian particle. Chiral active particles perform circular motions that give rise to slow transport at late times. By interrupting these circular trajectories at the right time by performing a tumble at the correct angle, we show that particles can enhance their diffusion. After deriving exact expressions for the orientational propagator and correlations, we use this to calculate the first two moments of displacement. For the effective diffusion coefficient, we study various optimal tumbling strategies. We show that under optimization of the tumbling rate, the case of symmetrically distributed tumbles always gives rise to enhanced diffusion, with an effective diffusion coefficient taking a universal value. Next, two cases are considered in detail, namely, directional reversal and tumbles at an arbitrary but fixed angle. We discuss how asymmetric tumbles can enhance diffusion beyond that of symmetric tumbles. Finally, we discuss a situation where the reorientations are realized dynamically in finite time.

DOI: [10.1103/PhysRevE.110.064606](https://doi.org/10.1103/PhysRevE.110.064606)

I. INTRODUCTION

Over recent decades, active matter has fascinated the nonequilibrium statistical physics and soft matter communities with a wide range of intricate phenomena [1–3]. By breaking time-reversal symmetry on the individual particle level, active systems are able to perform tasks such as self-propulsion by continuously absorbing and dissipating energy from and into the environment [4,5]. When parity symmetry is also broken on the particle scale, chiral motion tends to emerge, with circular trajectories of a fixed handedness characterizing the particle dynamics [6,7].

Chiral active motion is found in a wide array of systems ranging from bacteria swimming near surfaces [8–12] to synthetic self-propelled particles such as colloids or granular particles [13–16]. While their motion is intriguing and displays many nontrivial behaviors both on the single-particle and collective level [17–22], late-time effective diffusion is strongly suppressed compared with achiral motion [7]. Hence, chiral motion is by itself not a good strategy of motion if the goal is to increase the distance traversed in a given time. However, when chirality is present in the dynamics simultaneously with other modes of swimming, competing effects can appear.

Recently, it has become clear that strategic interruptions of chiral trajectories can strongly benefit late-time diffusive transport. In recent experiments investigating the motion of *Escherichia coli* near surfaces, it was seen that intermittent stops at a correct rate allow particles to optimize their diffusion [23]. Similarly, a reversal in the sign of the chirality at the correct time interrupts the circular swimming trajectories and gives rise to an effective diffusion coefficient with multiple

local maxima as the chirality is varied [24]. Furthermore, chirality in the presence of correlated noise can lead to enhanced diffusion [25,26]. In light of these findings, it is opportune to investigate strategic ways to abort circular trajectories to enhance spatial transport.

Here, we consider competing effects resulting from the simultaneous presence of both chirality and discrete tumbles in the motion of a self-propelled active Brownian particle (ABP) (see Fig. 1). We consider tumbling angles that follow any normalized probability density on the circle, symmetric or asymmetric. We fully characterize the directional correlations for the particle and provide exact expressions for both the first and second moments of displacement. Using these results, we consider several examples of tumbling strategies where the late-time effective diffusion coefficient can be optimized. After deriving a general expression for the optimal tumbling rate that maximizes the effective diffusivity, we consider two cases in detail: directional reversals and asymmetric tumbling strategies.

This paper is organized as follows: Section II provides the theoretical background of the model we consider, and derives a range of general results, including a general expression for the optimal tumbling rate. Section III considers the particular case of directional reversals, and Sec. IV deals with asymmetric tumbles. In Sec. V, we consider finite-time reorientations that dynamically realize the tumbling distributions, before a concluding discussion is offered in Sec. VI.

II. GENERAL THEORETICAL ASPECTS

Both chiral motion and run-and-tumble dynamics have a long history in statistical physics and fluids dynamics. Submerged bodies with circular trajectories have been studied for decades in the context of asymmetric particles in stationary or sheared liquids [27]. In the context of active matter,

*Contact author: kristian.olsen@hhu.de

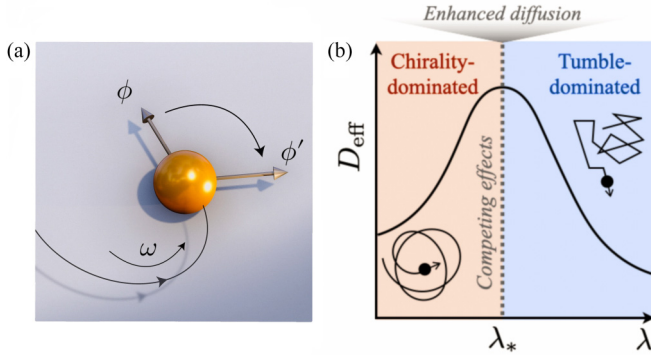


FIG. 1. (a) Active particles with a chirality ω perform random reorientations by tumbling an angle θ , drawn from a distribution $b(\theta)$. Tumbles take place at a constant rate λ . (b) When the rate of tumbling is either low ($\lambda \ll \lambda_*$) or high ($\lambda \gg \lambda_*$), transport is suppressed due to circular trajectories or rapid tumbles, respectively. For optimal rates $\lambda \approx \lambda_*$, enhanced diffusion takes place.

circular paths have been known to occur in the swimming patterns of a wide range of bacteria and other microorganisms, documented, for example, by Berg and Turner [28], but also mentioned in the notes of A. P. van Leeuwenhoek during his studies of *Animalicules* more than three centuries earlier [29]. From a theoretical perspective, however, chiral self-propelled motion is a relatively recent endeavor [6].

Tumbling motion also has a long and rich history. Movement in straight lines interrupted by directional switches in one dimension was a very simple way of generating random motion and has been studied in various forms over the last hundred years in the context of heat transport or random walks [30–33]. In the early 1970s, many new observations of *Escherichia coli* trajectories emerged, one famous study being that of Berg and Brown in 1972 [34]. A few years later, Lovely and Dahlquist presented a stochastic model of run-and-tumble motion in both two and three dimensions directly motivated by the recent experiments by Berg and Brown [35]. In particular, this is the earliest reference (to our knowledge) where transport properties under a general distribution of tumble angles were considered. Since then, various generalizations have been considered [36–49].

Here, we extend the conventional chiral ABP model by including tumbles where the reorientation angle follows a general distribution $b(\phi)$. Tumbles take place at a constant rate λ . The equations of motion take the form

$$\dot{\mathbf{x}} = v_0 \hat{e}(t) = v_0 [\cos \phi, \sin \phi] \quad (1)$$

$$\dot{\phi} = \sqrt{2D_r} \xi(t) + \omega + \sum_{\alpha} \theta_{\alpha} \delta(t - t_{\alpha}), \quad (2)$$

where $\{\theta_{\alpha}\}$ are random (independent) tumbling angles drawn from a distribution with density $b(\theta)$, and $\{t_{\alpha}\}$ is a sequence of random instances of time generated by a Poisson process with rate λ . In Eq. (2), D_r is the rotational diffusion coefficient, which determines the strength of the Gaussian white noise $\xi(t)$. The self-propulsion speed is given by v_0 , and ω is the chirality. See Fig. 1 for a sketch of the dynamics. The associated Fokker-Planck equation can be obtained by the probability

balance equation

$$p(\mathbf{x}, \phi, t + dt) = \lambda dt \langle p(\mathbf{x}, \phi - \theta, t) \rangle_{\theta} + (1 - \lambda dt) \langle p(\mathbf{x} - \Delta_{\mathbf{x}}, \phi - \Delta_{\phi}, t) \rangle_{\Delta_{\mathbf{x}}, \Delta_{\phi}} \quad (3)$$

where $\Delta_{\mathbf{x}} = v_0 dt \hat{e}(t)$ and $\Delta_{\phi} = \sqrt{2D_r} dW(dt)$ are infinitesimal steps associated with the stochastic dynamics *without* tumbles ($\lambda = 0$). The first term on the right-hand side comes from trajectories where a tumble took place in $(t, t + dt)$, which happens with probability λdt . In this case, the contributions to the propagator $p(\mathbf{x}, \phi, t + dt)$ comes from state-space points $(\mathbf{x}, \phi - \theta)$ that tumble into (\mathbf{x}, ϕ) . Similarly, the second term comes from trajectories with no tumble in $(t, t + dt)$, in which case the dynamics simply evolve according to the stochastic equations of motion with $\lambda = 0$.

Expanding in small dt , $\Delta_{\mathbf{x}}$, Δ_{ϕ} and letting $dt \rightarrow 0$ results in the Fokker-Planck equation

$$\begin{aligned} \partial_t p(\mathbf{x}, \phi, t) = & -v_0 \nabla_{\mathbf{x}} \cdot [\hat{e} p(\mathbf{x}, \phi, t)] + D_r \partial_{\phi}^2 p(\mathbf{x}, \phi, t) \\ & - \omega \partial_{\phi} p(\mathbf{x}, \phi, t) \\ & - \lambda p(\mathbf{x}, \phi, t) + \lambda \int d\theta b(\theta) p(\mathbf{x}, \phi - \theta, t) \end{aligned} \quad (4)$$

Similar composite dynamics with both rotational diffusion and tumble dynamics were studied in the 1990s by Schnitzer [36], but to the best of our knowledge, the combined effect of chirality and generalized tumbles with a distribution $b(\theta)$ has not been studied.

To build an intuition for the dynamics of this model before proceeding with a formal analysis, it is instructive to consider an expansion in small tumbling angles θ . We expand to the second order in the integrand

$$\begin{aligned} \int d\theta b(\theta) p(\mathbf{x}, \phi - \theta, t) \approx & p(\mathbf{x}, \phi, t) - \langle \theta \rangle \partial_{\phi} p(\mathbf{x}, \phi, t) \\ & + \frac{\langle \theta^2 \rangle}{2} \partial_{\phi}^2 p(\mathbf{x}, \phi, t) \end{aligned} \quad (5)$$

Combining this with the Fokker-Planck equation, we find the effective description

$$\begin{aligned} \partial_t p(\mathbf{x}, \phi, t) = & -v_0 \nabla_{\mathbf{x}} \cdot [\hat{e} p(\mathbf{x}, \phi, t)] \\ & + \left[D_r + \lambda \frac{\langle \theta^2 \rangle}{2} \right] \partial_{\phi}^2 p(\mathbf{x}, \phi, t) \\ & - [\omega + \lambda \langle \theta \rangle] \partial_{\phi} p(\mathbf{x}, \phi, t) \end{aligned} \quad (6)$$

We see that in the limit of small tumbling angles, the first-order correction shifts the chirality, while the second-order correction contributes to the angular diffusion. It is also worth noting that, in the case of symmetric tumbling distributions, all odd moments vanish, and there is no correction to the chirality.

From these equations, we see that the tumbling chiral ABP in the small tumbling angle limit behaves as a chiral ABP with renormalized parameters. The higher-order corrections to Eq. (5) have no analogy in the existing chiral ABP model and will introduce new terms in the equation. In the following, we provide an exact (nonperturbative) solution to the angular

dynamics and discuss the generalization of these small-angle results to the general case.

A. Angular propagator and correlation function

Many interesting observables can be calculated based on the knowledge of angular dynamics and correlations. Integrating the Fokker-Planck equation over space, we have the angular equation of motion

$$\begin{aligned} \partial_t \rho(\phi, t|\phi_0) &= D_r \partial_\phi^2 \rho(\phi, t|\phi_0) - \omega \partial_\phi \rho(\phi, t|\phi_0) \\ &\quad - \lambda \rho(\phi, t|\phi_0) + \lambda \int d\theta b(\theta) \rho(\phi - \theta, t|\phi_0), \end{aligned} \quad (7)$$

where $\rho(\phi, t|\phi_0) = \int d\mathbf{x} p(\mathbf{x}, \phi, t|\mathbf{x}_0, \phi_0)$ is the marginalized angular propagator. We also used the fact that the angular dynamics is not coupled to the spatial dynamics, implying that $\rho(\phi, t|\mathbf{x}_0, \phi_0) = \rho(\phi, t|\phi_0)$. This equation can conveniently be solved by Fourier series. We write

$$\rho(\phi, t|\phi_0) = \sum_{n=-\infty}^{\infty} \tilde{\rho}_n(t|\phi_0) e^{-in\phi}, \quad (8)$$

where the Fourier coefficients are given by

$$\tilde{\rho}_n(t|\phi_0) = \frac{1}{2\pi} \int_{-\pi}^{\pi} d\phi \rho(\phi, t|\phi_0) e^{in\phi}. \quad (9)$$

The Fokker-Planck equation then gives an equation of motion for the coefficients as

$$\begin{aligned} \partial_t \tilde{\rho}_n(t|\phi_0) &= [-D_r n^2 + i\omega n - \lambda + 2\pi \lambda \tilde{b}_n] \tilde{\rho}_n(t|\phi_0) \\ &= -\mu_n \tilde{\rho}_n(t|\phi_0), \end{aligned} \quad (10)$$

where we defined

$$\mu_n \equiv D_r n^2 - i\omega n + \lambda(1 - 2\pi \tilde{b}_n). \quad (12)$$

These numbers μ_n , which may be real or complex, determine the dynamics of the particle's direction of motion. In Eq. (12), we also used the Fourier series of the tumbling angle density

$$b(\phi) = \sum_{n=-\infty}^{\infty} \tilde{b}_n e^{-in\phi}. \quad (13)$$

In total, we then have the angular propagator

$$\rho(\phi, t|\phi_0) = \frac{1}{2\pi} \sum_{n=-\infty}^{\infty} e^{-\mu_n t} e^{-in(\phi-\phi_0)}, \quad (14)$$

where we used a Dirac delta function at $\phi = \phi_0$ as the initial condition. We observe that μ_n has the property $\mu_n^* = \mu_{-n}$, which ensures that $\rho(\phi, t|\phi_0)$ is real. This follows from the fact that the same property holds for the tumbling distribution (i.e., $\tilde{b}_n^* = \tilde{b}_{-n}$). Additionally, we observe that the angular propagator has a homogeneity property $\rho(\phi, t|\phi_0) = \rho(\phi - \phi_0, t|0)$.

Combining these equations, one readily finds the angular correlation function $\mathcal{C}(t' - t) = \langle \hat{e}(t') \cdot \hat{e}(t) \rangle$ by the integral

$$\begin{aligned} \mathcal{C}(t' - t) &= \int d\phi d\phi' \cos(\phi' - \phi) \rho(\phi', t'|\phi) \rho(\phi, t|\phi_0) \\ &= \frac{e^{-\mu_1(t'-t)} + e^{-\mu_{-1}(t'-t)}}{2}. \end{aligned} \quad (15)$$

(16)

By using the fact that $\mu_{-1} = \mu_1^*$ we can write

$$\mathcal{C}(t' - t) = \frac{e^{-\mu_1(t'-t)} + e^{-\mu_1^*(t'-t)}}{2}. \quad (17)$$

Since $\mu_1 \in \mathbb{C}$ is, in general, a complex number, we decompose it into real and imaginary parts, leading to

$$\mathcal{C}(t' - t) = e^{-\text{Re}[\mu_1](t'-t)} \cos(\text{Im}[\mu_1](t'-t)). \quad (18)$$

When there are no tumbles ($\lambda = 0$), we have $\text{Re}[\mu_1] = D_r$ and $\text{Im}[\mu_1] = -\omega$, and we recover the standard results for chiral active particles. Based on this analogy, we define an effective persistence time and an effective chirality that takes into account the effect of tumbles:

$$\tau_{\text{eff}}^{-1} \equiv \text{Re}[\mu_1] = D_r + \lambda - \lambda \int_{-\pi}^{\pi} d\theta b(\theta) \cos(\theta) \quad (19)$$

$$\omega_{\text{eff}} \equiv -\text{Im}[\mu_1] = \omega + \lambda \int_{-\pi}^{\pi} d\theta b(\theta) \sin(\theta). \quad (20)$$

We notice that the effective persistence time, which governs the exponential decay of the correlation function, gets a contribution from the symmetric part of the tumbling density. Likewise, the effective chirality, which governs the oscillatory part of the correlation function, only gets a contribution from tumbles when the tumbling angle density has an antisymmetric component. Finally, we note as a matter of consistency that for the second order expansion in the tumbling angle, these effective parameters coincide with those in Eq. (6).

It is worth emphasizing that, in strong contrast to the conventional chiral ABP case, the effective persistence and chirality are no longer always independent parameters, and competing effects may arise. For example, trying to minimize the effective chirality so that trajectories become maximally rectilinear may also cause a significant decrease in the effective persistence time, making the trajectories noisy and irregular. Even when tumbles are symmetric and $\omega_{\text{eff}} = \omega$, tumbles can disrupt circular particle trajectories and strongly affect the dynamics. These effects will be important later when we discuss the effective diffusion coefficient of this model under various tumbling strategies.

B. Mean displacement

Before considering the mean-squared displacement and transport properties, we consider the mean displacement. We consider a fixed initial orientation ϕ_0 . We then have

$$\langle \hat{\mathbf{x}} \rangle = v_0 \langle \hat{e}(t) \rangle = v_0 \langle e^{i\phi(t)} \rangle \quad (21)$$

where we have identified the two-dimensional vector with a complex number. We have

$$\langle e^{i\phi(t)} \rangle = \int_{-\pi}^{\pi} d\phi e^{i\phi} \rho(\phi - \phi_0, t). \quad (22)$$

Changing the integration variable to $\vartheta = \phi - \phi_0$, we have

$$\langle e^{i\phi(t)} \rangle = e^{i\phi_0} \int_{-\pi}^{\pi} d\vartheta e^{i\vartheta} \rho(\vartheta, t) = e^{i\phi_0 - \mu_1 t}. \quad (23)$$

The spatial components of the mean displacement can then be obtained as real and imaginary parts of this complex

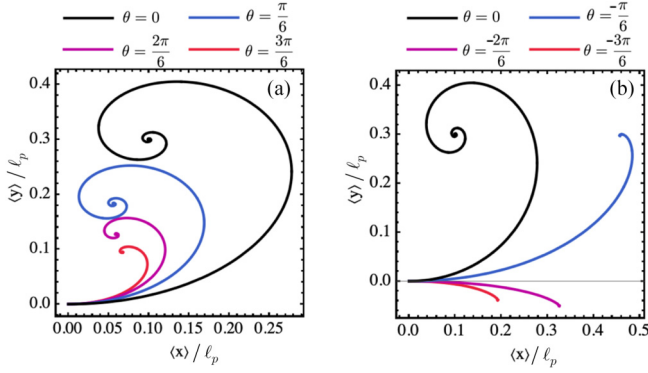


FIG. 2. Mean position of the particle under asymmetric tumbles at an angle θ , measured in units of the persistence length $\ell_p = v_0/D_r$. Panel (a) shows positive angles while panel (b) shows the corresponding negative tumbling angles. Parameters are set to $D_r = 1$, $v_0 = 1$, $\phi_0 = 0$, $\lambda = 4$, $\omega = 3$.

exponential, which leads to

$$\langle \dot{\mathbf{x}} \rangle = v_0 e^{-t/\tau_{\text{eff}}} \begin{bmatrix} \cos(\omega_{\text{eff}} t + \phi_0) \\ \sin(\omega_{\text{eff}} t + \phi_0) \end{bmatrix} \quad (24)$$

The mean position can then be obtained simply by integration

$$\langle \mathbf{x}(t) \rangle = \int_0^t dt' \langle \dot{\mathbf{x}}(t') \rangle \quad (25)$$

As in the case of a pure chiral ABP, the mean displacement is a *spira mirabilis*, where now the additional tumbling events determine the overall shape of the spiral. Figure 2 shows some of these spirals for the case $b(\phi) = \delta(\phi - \theta)$.

$$\langle \mathbf{x}^2(t) \rangle = \frac{2v_0^2 \tau_{\text{eff}}}{1 + \tau_{\text{eff}}^2 \omega_{\text{eff}}^2} t + \frac{2\tau_{\text{eff}}^2 v_0^2 (\tau_{\text{eff}}^2 \omega_{\text{eff}}^2 - 1)}{(1 + \tau_{\text{eff}}^2 \omega_{\text{eff}}^2)^2} + \frac{2v_0^2 \tau_{\text{eff}}^2 e^{-\frac{t}{\tau_{\text{eff}}}} [\cos(\omega_{\text{eff}} t) (\tau_{\text{eff}}^2 \omega_{\text{eff}}^2 - 1) + 2\tau_{\text{eff}} \omega_{\text{eff}} \sin(\omega_{\text{eff}} t)]}{(1 + \tau_{\text{eff}}^2 \omega_{\text{eff}}^2)^2} \quad (28)$$

When tumbles are symmetric, $\omega_{\text{eff}} = \omega$ from Eq. (20). The mean-squared displacement then only depends on the tumbling distribution through $\int d\phi b(\phi) \cos \phi$, which is related to the first Fourier mode of the density $b(\phi)$. This has been shown for achiral tumblers with a symmetric tumbling distribution in the past, that is, by Taktikos *et al.* [51] and even earlier in the 1970s by Lovely and Dahlquist [35]. Since we also allow asymmetric tumbling distributions, an additional dependence on $\int d\phi b(\phi) \sin \phi$ appears in the general case.

At late times, the effective diffusivity is calculated as

$$D_{\text{eff}} \equiv \lim_{t \rightarrow \infty} \frac{\langle \mathbf{x}^2(t) \rangle}{2t} \quad (29)$$

By using the mean-squared displacement, Eq. (28), we find

$$D_{\text{eff}}(\lambda; [b(\phi)]) = v_0^2 \frac{\tau_{\text{eff}}^{-1}(\lambda; [b(\phi)])}{\tau_{\text{eff}}^{-2}(\lambda; [b(\phi)]) + \omega_{\text{eff}}^2(\lambda; [b(\phi)])}. \quad (30)$$

Several things are worth noting. First, we note that by construction [through Eqs. (18)–(20)], this takes a similar-looking form to the normal chiral ABP case. However, it is worth

It is also worth noting that even in the absence of noise ($D_r = 0$), there can never be a tumbling strategy that results in linear motion, and from the previous one can show that $\langle x_i(t) \rangle / t \rightarrow 0$ at late times for any tumbling strategy. This is likely different for non-Poissonian tumbling protocols, where one can imagine, for example, a particle with deterministic directional reversals exactly after a half circle has been spanned, leading to a linear skipping motion. For Poissonian reorientations, this is never the case.

C. Mean-squared displacement

The mean-squared displacement contains much information regarding the dynamics of the system and is one of the most studied quantities for active single-particle dynamics [50]. Since we know that the first moment of the displacement is always constant at late times, the mean-squared displacement gives the variance of the particle density at late times. Furthermore, if we consider an ensemble where the initial orientation ϕ_0 is random and uniformly distributed on the circle $[-\pi, \pi]$, $\langle \mathbf{x}(t) \rangle = 0$ at all times. The mean-squared displacement is calculated from the correlations of the orientation vector $\hat{e}(t)$:

$$\langle \mathbf{x}^2(t) \rangle = v_0^2 \int_0^t dt' \int_0^t dt'' \langle \hat{e}(t') \cdot \hat{e}(t'') \rangle \quad (26)$$

$$= v_0^2 \int_0^t dt' \int_0^t dt'' \mathcal{C}(t', t''), \quad (27)$$

where the orientational correlation function is $\mathcal{C}(t', t'') = \langle \cos[\phi(t') - \phi(t'')] \rangle$. From Eqs. (18)–(20) we find the mean-squared displacement

emphasizing that the dynamics leading to this diffusion coefficient are completely different; the previous formula gives the effective diffusion coefficient for any distribution of tumbling angles $b(\theta)$ and tumbling rate λ . We emphasize the D_{eff} depends parametrically on the tumbling rate (as well as on model parameters such as rotational diffusion, self-propulsion speed, and chirality) and depends functionally on the tumbling angle distribution $b(\theta)$ through its Fourier coefficients. Secondly, Ref. [23] considers a model for intermittent stop-and-go motion of chiral bacteria near surfaces. In this case, after a stop, it was assumed that the particle reorients by an angle distributed with a Heaviside function. In the limit where the stops are instantaneous and the same tumbling distribution is used, we find agreement between Eq. (30) and the results of Ref. [23]. Finally, the special case of uniform tumbles $b(\phi) = (2\pi)^{-1}$ can be recovered by the methods presented in Ref. [52], where a general framework for predicting effective transport coefficients under symmetric stop-and-go processes was developed. Tumbles in this case correspond to instantaneous stop-and-go events. However, the results presented here are far more general, as we can study optimal reorientation strategies for any $b(\phi)$.

D. Optimal tumbling rates

From the effective diffusion coefficient, Eq. (30), we can derive a general expression for the optimal rate of tumbling, λ_* , that maximizes the diffusivity for any tumbling dynamics $b(\theta)$. As a matter of notation, we recall that the effective persistence time and effective chirality depend on the tumbling rate through

$$\tau_{\text{eff}}^{-1} = D_r + \lambda - 2\pi\lambda\text{Re}[\tilde{b}_1] \quad (31)$$

$$\omega_{\text{eff}} = \omega + 2\pi\lambda\text{Im}[\tilde{b}_1], \quad (32)$$

where we by $\text{Re}[\tilde{b}_1]$ and $\text{Im}[\tilde{b}_1]$ denote the real and imaginary parts of the first Fourier coefficient of the tumbling density. By differentiating with respect to the rate, we can identify the optimal tumbling rate through $\partial_{\lambda_*} D_{\text{eff}}(\lambda_*) = 0$. After simplifying the algebra, we find

$$\lambda_* = \frac{\sqrt{\frac{[2\pi D_r \text{Im}[\tilde{b}_1] + \omega(2\pi \text{Re}[\tilde{b}_1] - 1)]^2}{(2\pi \text{Im}[\tilde{b}_1])^2 + (2\pi \text{Re}[\tilde{b}_1] - 1)^2}} - D_r}{1 - 2\pi \text{Re}[\tilde{b}_1]}. \quad (33)$$

This only exists when the resulting λ_* is positive. Intuitively, an optimal tumbling rate should interrupt the circular trajectories at optimal moments in time, resulting in a more persistent trajectory. We see that the optimal tumbling rate is determined not only by the noise D_r , but also depends on the specific tumbling dynamics used to interrupt the circular paths, which are encoded in the distribution $b(\theta)$.

E. Universal maximum in the case of symmetric tumbles

In the case of symmetric tumbles, $\text{Im}[\tilde{b}_1] = 0$, and the expression for the optimal tumbling rate simplifies drastically:

$$\lambda_* = \frac{|\omega| - D_r}{1 - 2\pi \text{Re}[\tilde{b}_1]}. \quad (34)$$

We see that a positive solution only exists if $|\omega| > D_r$. The effective diffusion coefficient in this case can, through Eq. (30), be shown to take the compact form

$$D_{\text{eff}} = \frac{v_0^2}{2|\omega|}. \quad (35)$$

We emphasize that this maximum value is universal in the sense that it is independent of the exact tumbling dynamics $b(\theta)$ and the rotational noise.

For the sake of further intuition regarding this result, we note that the effective persistence time τ_{eff} and effective chirality ω_{eff} are independent in this case, since $\omega_{\text{eff}} = \omega$ is independent of the tumbling distribution. Hence, the effective diffusivity

$$D_{\text{eff}} = \frac{v_0^2 \tau_{\text{eff}}^{-1}}{\tau_{\text{eff}}^{-2} + \omega^2} \quad (36)$$

can be maximized by finding the optimal value of τ_{eff} , independently of what the exact tumbling dynamics are. This optimal effective persistence time is $\tau_{\text{eff}} = |\omega|^{-1}$, which occurs exactly when the tumbling rate takes the form given in Eq. (34). Since this statement is independent of the tumbling dynamics, it also holds for the case of no tumbles; in other words, if one could somehow tune the rotational noise

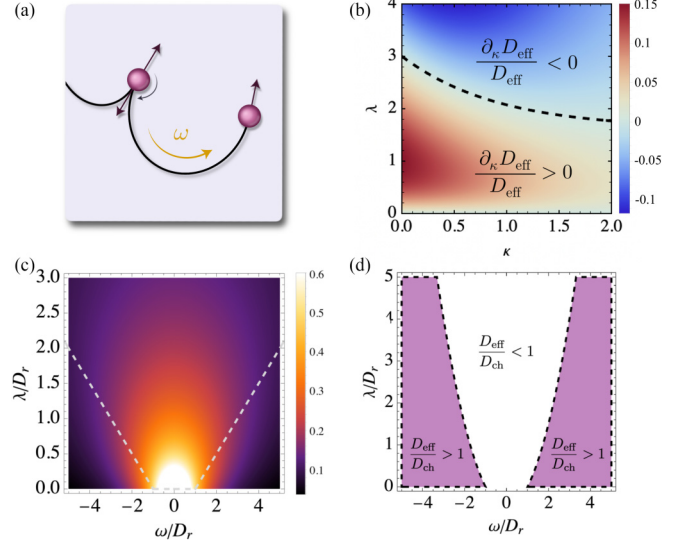


FIG. 3. (a) An active particle with chirality ω and directional reversals at random times with rate λ . (b) Slope of the effective diffusivity as a function of reversal rate and reversal accuracy, showing domains of positive and negative slope. (c) Effective diffusion coefficient as a function of rescaled chirality ω/D_r and reversal rate λ/D_r . The color bar indicates the value of the effective diffusivity measured relative to the diffusivity v_0^2/D_r of a normal active Brownian particle. The dashed gray line shows the optimal rate λ_* for fixed ω . Parameters used are $D_r = 1$, $v_0 = 1$. (d) Effective diffusion coefficient measured relative to the case of pure chiral motion ($\lambda = 0$). Shaded areas show parameter space regions where reversals benefit the exploration and give rise to diffusivity that is greater than that of pure chiral motion.

strength D_r , the maximal diffusion coefficient D_{ch} of a chiral ABP is also given by Eq. (35). The noise giving rise to D_r is externally imposed and often not controllable. Regardless, this formal argument shows that, for any tumbling dynamics, $D_{\text{eff}}(\lambda_*) \geq D_{\text{ch}}$ at any fixed value of D_r , and the inequality is only attained under the fine-tuning $D_r = |\omega|$. Hence, symmetric tumbles of any type can always be optimized to give rise to enhanced diffusion, and the value of the optimal diffusivity is universally given by Eq. (35).

While it is not generally true that asymmetric tumbles always lead to enhanced diffusion, we will show with an example in section IV that for certain tumbling angles, diffusion can be enhanced beyond that of Eq. (35).

III. DIRECTIONAL REVERSALS

The first of two examples we consider in more detail is the case where the tumbles give rise to reversals in the particle's direction of motion [see Fig. 3(a)]. Such behavior is well known to be a part of the swimming patterns of many microorganisms [53–58]. The effect of reversals in the absence of chirality has been studied from a theoretical perspective in recent years, including dynamical properties of particles in free space and confinement [44,59–61], as well as collective effects [62].

If the reversals were perfectly precise, we would have $b(\theta) = \delta(\theta - \pi)$. However, real-world reversals are often im-

perfect and will not always take place at a turning angle of 180° . For example, Ref. [57] reports that among a range of marine bacteria that perform reversals, more than 70% turn at an angle greater than 150° . To model such imperfect reversals, we consider a distribution of tumbling angles of the von Mises type

$$b(\theta) = \frac{1}{2\pi I_0(\kappa)} \exp[\kappa \cos(\theta - \pi)], \quad (37)$$

which behaves similarly to a Gaussian on a circle, in this case with a peak at $\theta = \pi$. In Eq. (37), $I_n(z)$ is a modified Bessel function of the first kind. The parameter κ determines the width of the distribution, with a Dirac delta-peak resulting in the $\kappa \rightarrow \infty$ limit. Conversely, when $\kappa \rightarrow 0$, conventional tumbling with uniformly distributed tumbling angles will be recovered. We refer to κ as the reversal precision.

To use Eqs. (30) and (34) to find the diffusivity and optimal tumbling angle in the presence of chirality, we need the quantity $\text{Re}[\mu_1]$, while $\text{Im}[\mu_1] = -\omega$ since the tumbling distribution in this case is symmetric. $\text{Re}[\mu_1]$ is, in this case, given by $\text{Re}[\tilde{b}_1]$, which we can calculate to be

$$2\pi \text{Re}[\tilde{b}_1] = \int_{-\pi}^{\pi} d\theta \frac{1}{2\pi I_0(\kappa)} \exp[\kappa \cos(\theta - \pi)] \cos \theta \quad (38)$$

$$= -\frac{I_1(\kappa)}{I_0(\kappa)}. \quad (39)$$

This gives the effective diffusivity and associated optimal tumbling rate

$$D_{\text{eff}} = v_0^2 \frac{D_r + \lambda + \lambda \frac{I_1(\kappa)}{I_0(\kappa)}}{\left(D_r + \lambda + \lambda \frac{I_1(\kappa)}{I_0(\kappa)}\right)^2 + \omega^2}, \quad (40)$$

$$\lambda_* = \frac{|\omega| - D_r}{1 + \frac{I_1(\kappa)}{I_0(\kappa)}}. \quad (41)$$

It is worth emphasizing that the factor $\frac{I_1(\kappa)}{I_0(\kappa)}$ is a simple monotonically increasing function interpolating between zero and unity as κ is increased. The optimal tumbling rate λ_* is therefore also monotonic and always decreasing as a function of κ . This implies that to move optimally, the particle has to tumble less frequently if there is a high precision in the reversals.

One may take into account the various costs associated with sudden reorientations. For example, it is known that the energetic cost of a tumble depends crucially on the details of the reorientation, that is, whether the bacteria body has to rotate or if simply the flagella, reverse, their rotational direction [63]. Alternatively, reorientations take finite time, and this time overhead can be thought of as a hidden cost associated with each reversal [64]. The ability to optimize diffusion by performing fewer but more precise reversals can then benefit the accumulated cost. However, if higher reversal precision for some reason were to come at a higher cost, a trade-off would appear, and it may be optimal for the particle to sacrifice precision in favor of lower reversal costs. Whatever the situation may be, the optimized diffusion coefficient, taking the universal value given in Eq. (35), is independent of the reversal precision κ , which can hence be tuned freely without motility losses.

The effective diffusion coefficient behaves less trivially as the reversal accuracy κ is varied when $\lambda \neq \lambda_*$. Figure 3(b)

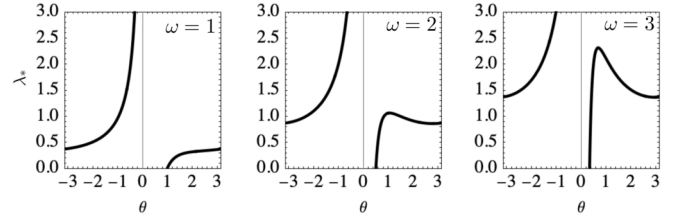


FIG. 4. Optimal tumbling rate λ_* for a chiral active Brownian particle with asymmetric tumbles as a function of the tumbling angle θ . Panels correspond to different values of the chirality ω as indicated. The remaining parameters are set to $D_r = 0.25$, $v_0 = 1$.

shows a plot over the parameter space (κ, λ) of the slope $\partial_\kappa D_{\text{eff}}(\kappa, \lambda)$, showing clear regions of positive and negative slope. The dashed line shows the $\lambda_*(\kappa)$ line, separating the two regions. For reversal rates $\lambda < \lambda_*(\infty)$, the effective diffusion coefficient always increases monotonically as a function of κ , while for $\lambda > \lambda_*(0)$, the effective diffusion coefficient decays monotonically as a function of κ . For intermediate reversal rates $\lambda \in (\lambda_*(\infty), \lambda_*(0))$, there is a nonmonotonic behavior as the precision κ is varied, which in Figure 3(b) is seen from the fact that the dashed line is crossed as κ is varied for reversal rates in this range.

Figure 3(c) shows the effective diffusion coefficient D_{eff} as a function of (rescaled) reversal rate λ and (rescaled) chirality ω for $\kappa \rightarrow \infty$ (e.g., perfect reversal). For fixed ω , the optimal rate $\lambda_* = (|\omega| - D_r)/2$ is shown in a dashed line. Figure 3(d) shows a related phase diagram plot displaying the regions where the effective diffusion coefficient is greater or lesser than the tumble-free case. We see that, generically, transport can be enhanced by tumbles when chirality is large.

IV. ASYMMETRIC TUMBLES

Next, we consider the case where the particle tumbles at an arbitrary angle θ , that is, $b(\phi) = \delta(\phi - \theta)$. In contrast to directional reversals, these asymmetric tumbles introduce an effective chirality, as has, for example, been observed in a model of a tumble that only moves in four principal directions with asymmetric tumbling rates [65], and for discrete random walkers that turn at a fixed angle every step [66]. In the present case, we have

$$\tau_{\text{eff}}^{-1} = D_r + \lambda[1 - \cos(\theta)] \quad (42)$$

$$\omega_{\text{eff}} = \omega + \lambda \sin(\theta). \quad (43)$$

From Eqs. (30) and (33), we have the diffusivity and associated optimal rate

$$D_{\text{eff}} = v_0^2 \frac{D_r + \lambda - \lambda \cos \theta}{(D_r + \lambda - \lambda \cos \theta)^2 + (\omega + \lambda \sin \theta)^2} \quad (44)$$

$$\lambda_* = \frac{D_r}{\cos \theta - 1} + \frac{|\omega(\cos \theta - 1) + D_r \sin \theta|}{\sqrt{2}[1 - \cos \theta]^{3/2}}. \quad (45)$$

We note that the optimal rate does not exist for all choices of ω and θ , and is considered to exist only when this expression is positive. Figure 4 shows the optimal tumbling rate as a function of the tumbling angle θ , for different values of the chirality ω . We see that typically, there exists a small range of tumbling angles near $\theta = 0$ for which there is no optimal

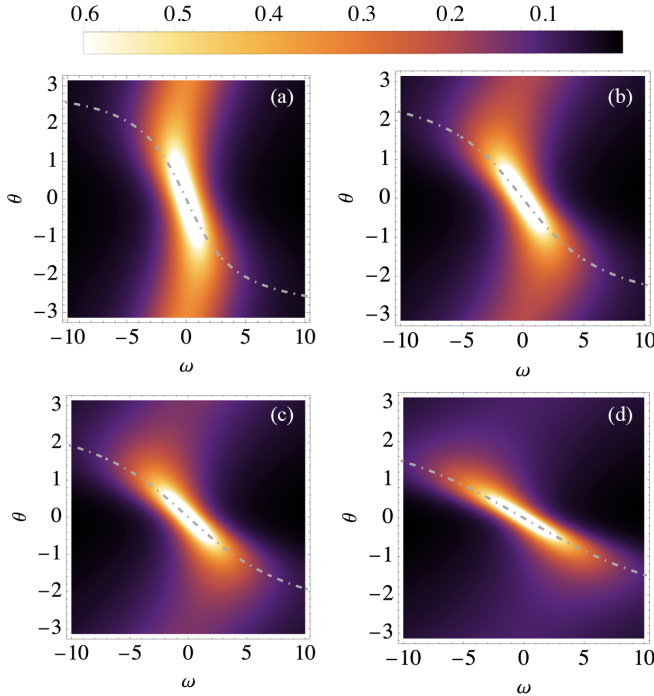


FIG. 5. Effective diffusion coefficient as a function of chirality ω and tumbling angle θ . Panels (a)–(d) show plots for $\lambda = 1, 2, 3, 5$, respectively. Dashed gray lines show the optimal tumbling angle θ for fixed chirality ω . The color bar indicates the value of the effective diffusivity measured relative to the diffusivity v_0^2/D_r of a normal active Brownian particle. Parameters are set to $D_r = v_0 = 1$.

tumbling rate. In these cases, the tumbles can never give rise to enhanced diffusion.

The diffusion coefficient can also be optimized with respect to the tumbling angle θ . Keeping the tumbling rate fixed, we find a maximized diffusivity when

$$\partial_\theta D_{\text{eff}} \sim (2\lambda D_r + D_r^2 - \omega^2) \sin \theta + 2\omega(D_r + \lambda) \cos \theta - 2\lambda\omega = 0. \quad (46)$$

This can conveniently be turned into a polynomial equation by utilizing trigonometric half-angle identities

$$\cos \theta = \frac{1 - z^2}{1 + z^2}; \quad \sin \theta = \frac{2z}{1 + z^2}, \quad (47)$$

where $z = \tan(\theta/2)$. Combining these equations then yields $z = \omega/(D_r + 2\lambda)$. Hence, the optimal tumbling angle is given by

$$\theta_* = -2 \tan^{-1} \left(\frac{\omega}{D_r + 2\lambda} \right). \quad (48)$$

Figure 5 shows the effective diffusion coefficient as a function of (ω, θ) together with the optimal tumbling angle θ_* for fixed ω in dashed lines for various values of the tumbling rate. We see that, generally, a positive chirality is associated with a negative optimal tumbling angle. This can be interpreted to mean that the tumbles try to counteract the chirality, making the particle trajectories as linear as possible. However, this intuitive picture only holds in the limit of frequent tumbling angles and low angular noise.

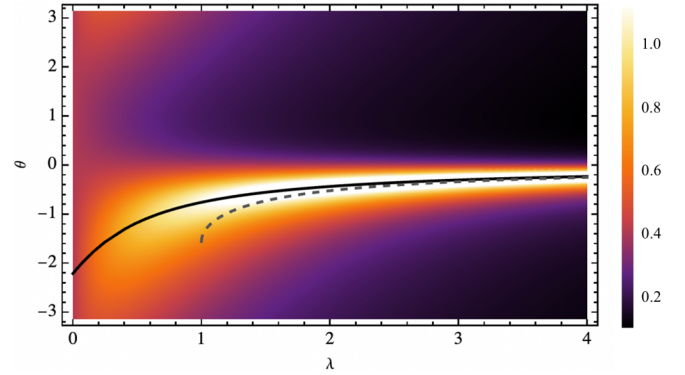


FIG. 6. Effective diffusion coefficient as a function of tumbling rate λ and tumbling angle θ . The color bar indicates the value of the effective diffusivity measured relative to the diffusivity v_0^2/D_r of a normal active Brownian particle. The black solid line corresponds to the optimal tumbling angle for fixed rate [Eq. (48)]. The dashed line shows the tumbling angle that makes the effective chirality ω_{eff} vanish, that is, $\tilde{\theta} = \sin^{-1}(-\omega/\lambda)$, valid only when the argument is greater than unity. Parameters are set to $D_r = 1/2, v_0 = 1, \omega = 1$.

To better see this, consider the tumbling angle for which $\omega_{\text{eff}} = 0$. This is simply $\tilde{\theta} = \sin^{-1}(-\omega/\lambda)$, which, in general, is not equal to the optimal tumbling angle we previously derived. However, this angle has a Taylor series, which coincides with θ_* at first order in λ^{-1} . Indeed, expanding the $\sin^{-1}(x) = x + \dots$ we have at large rates $\tilde{\theta} \approx -\omega/\lambda$. Similarly, Eq. (48) to first order takes the form $\theta_* \approx -\frac{2\omega}{D_r + 2\lambda}$. When $D_r \ll 2\lambda$, we can further approximate $\theta_* \approx -\frac{\omega}{\lambda}$. Figure 6 shows the diffusivity as a function of (θ, λ) , together with the optimal tumbling angle and the tumbling angle that eliminates the effective chirality. In the regime of large tumbling rates, we can use $\theta_* \approx -\frac{\omega}{\lambda}$ and expand D_{eff} to leading order, in which case we find $D_{\text{eff}} \approx v_0^2/D_r$, which is the diffusivity of a linear ABP. Hence, asymmetric tumbles can counteract the effect of chirality and give rise to a diffusivity that, at most, can take the value of a normal ABP.

V. DYNAMICAL REALIZATION OF REORIENTATIONS

Finally, we present a scenario where the distribution of reorientation angles $b(\theta)$ is realized dynamically rather than assumed *ad hoc*. We consider a model for intermittent active motion, where the particle stochastically switches between an active mobile phase and an immobile phase. During the immobile phase, no translational motion is generated, while the particle's orientation follows a dynamics similar to that of a chiral ABP (see Fig. 7). While such models for intermittent motion have been studied for decades [67,68], recent years has seen a renewed interest in the topic [42,69–76].

The immobile phases may be seen as a finite-time tumble event [69,75], where the distribution of tumbling angles depends on the duration of the immobile phase. In particular, if a particle enters one of the immobile phases at time t and leaves it at a time $t = t' + \tau$, we will assume the duration of stops to be drawn from a distribution with density $\psi_S(\tau)$. The particle's orientation will in this time evolve according to

$$\phi(t) = \phi(t') + \theta(\tau), \quad (49)$$

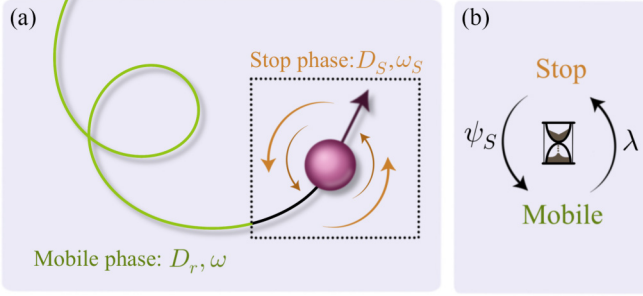


FIG. 7. (a) Intermittent active motion consists of mobile phases and immobile (“stop”) phases. During the two, the angular dynamics of the particle may, in general, be different. (b) The particle transitions from a mobile phase to a stop phase with rate λ . The stop phases have durations drawn from $\psi_S(\tau)$.

where the increment $\theta(\tau)$ is independent of the absolute time and only depends on the duration of the stop. The explicit dynamics are those of a chiral ABP with chirality ω_S and rotational diffusion coefficient D_S , such that the increments are distributed according to

$$b(\theta) = \int_0^\infty d\tau \psi_S(\tau) \frac{\exp\left(-\frac{(\theta - \omega_S \tau)^2}{4D_S \tau}\right)}{\sqrt{4\pi D_S \tau}}. \quad (50)$$

Here, it is assumed that the dynamics in the immobile phase, in general, may differ from those of the mobile phase.

Since the tumbles in this scenario have a finite duration, we must also rescale the mean-squared displacement accordingly, since Eq. (30) assumes instantaneous tumbles. To proceed, it is beneficial to temporarily work in an ensemble of a fixed number of immobile phases. A similar line of reasoning, whereby turning to a fixed- n ensemble simplified calculations, has been used both in stochastic resetting and run-and-tumble processes in the past [45,77–82]. Indeed, in an ensemble of fixed number n of immobile phases, or tumbles, the mean-squared displacement asymptotically behaves as

$$\langle \mathbf{x}^2(n) \rangle_{\text{inst.}} \approx 2D_{\text{eff}}^{(\text{inst.})} t_n = 2D_{\text{eff}}^{(\text{inst.})} \langle \tau_m \rangle n, \quad (51)$$

where n mobile phases take a time $\langle \tau_m \rangle n$ when the immobile phases are instant. Here, each mobile phase has a mean duration $\langle \tau_m \rangle = 1/\lambda$. However, since no motion is generated in the immobile phases by definition, this fixed- n mean-squared displacement (with fixed reorientation angles) must be the same even if the immobile phases had a duration τ_S . In this case, however, the mean observation time is given by $t_n = n(\langle \tau_S \rangle + \langle \tau_m \rangle)$. This leads to a rescaled mean-squared displacement when the immobile phases have finite durations

$$\langle \mathbf{x}^2(n) \rangle = 2 \frac{\langle \tau_m \rangle D_{\text{eff}}^{(\text{inst.})}}{\langle \tau_S \rangle + \langle \tau_m \rangle} t_n \quad (52)$$

Hence for finite-time tumbles, we expect the effective diffusion coefficient to be simply rescaled as

$$D_{\text{eff}} = \frac{\langle \tau_m \rangle}{\langle \tau_S \rangle + \langle \tau_m \rangle} D_{\text{eff}}^{(\text{inst.})}. \quad (53)$$

We see that to calculate the effective transport at late times for dynamically realized reorientations, Eq. (53), we need

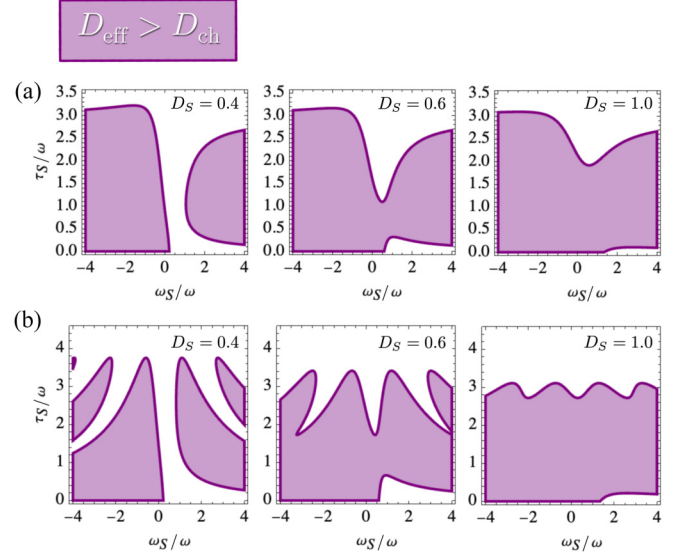


FIG. 8. Phase diagrams showing where diffusion is enhanced due to intermittent reorientations. (a) Exponential density $\psi_S(\tau) = \exp(-\tau/\tau_S)/\tau_S$, for three values of D_S . (b) Dirac delta density $\psi_S(\tau) = \delta(\tau - \tau_S)$, for three values of D_S . Other parameters are set to $\omega = 1$, $D_r = 1/4$, $\langle \tau_m \rangle = \lambda^{-1} = 5$.

only the diffusion coefficient for instantaneous reorientations $D_{\text{eff}}^{(\text{inst.})}$, given by Eq. (30), together with the distribution of reorientation angles, Eq. (50). The effective persistence time and effective chirality characterizing the reorientations from Eq. (50) can in this case be shown to take the form

$$\begin{aligned} \tau_{\text{eff}}^{-1} &= D_r + \lambda - \lambda \int_0^\infty d\tau \psi_S(\tau) e^{-D_S \tau} \cos(\omega_S \tau) \\ &= D_r + \lambda - \lambda \text{Re}[\tilde{\psi}_S(D_S - i\omega_S)] \end{aligned} \quad (54)$$

$$\begin{aligned} \omega_{\text{eff}} &= \omega + \lambda \int_0^\infty d\tau \psi_S(\tau) e^{-D_S \tau} \sin(\omega_S \tau) \\ &= \omega + \lambda \text{Im}[\tilde{\psi}_S(D_S - i\omega_S)], \end{aligned} \quad (55)$$

where $\tilde{\psi}_S$ is the Laplace transform of the density of stopping durations. In the absence of chirality in either of the two phases (i.e., $\omega = \omega_S = 0$), a complementary approach based on the velocity-correlation functions of intermittent active particles was recently studied in Ref. [69].

Figure 8 shows phase diagrams over the chirality and duration of the immobile phases (ω_S, τ_S), where shaded regions indicate diffusion enhancement (i.e. $D_{\text{eff}} \geq D_{\text{ch}}$). Figure 8(a) considers exponentially distributed immobile durations, with fixed mean τ_S . Figure 8(b) considers Dirac delta distributed immobile durations, with duration τ_S . Common to all cases is the fact that stops have to be sufficiently short but diffusion enhanced. Furthermore, when the chirality in the stop phase has the same sign as in the mobile phase, we see that the durations of the stops also have to be sufficiently long. We also note that, in the case of deterministic stopping times, Fig. 8(b), there is a strong re-entrant behavior as τ_S is varied for small values of D_S . This comes from the fact that an optimal reorientation angle can be achieved by performing

an additional complete rotation, which is possible only if the noise is sufficiently small.

VI. DISCUSSION

The dynamics of active particles under the simultaneous influence of chirality and tumbling dynamics were considered. We derived exact expressions for the angular probability density function, as well as for the corresponding correlation function. We found that while normally rotational diffusion determines the exponential decay rate of the correlations while chirality sets the oscillatory parts, the presence of tumbles couples these two effects. Effective transport properties have been investigated, and various tumbling strategies that maximize the effective diffusion coefficient have been identified.

For symmetric tumble distributions, we showed that the diffusion coefficient can always be optimized to give rise to enhanced diffusion relative to the pure chiral case. The value of the diffusion coefficient at optimality is universal, and is independent of the detail of the tumbles.

For asymmetric tumbles, the tumbles can be tuned to counteract the effect of the underlying chirality, giving rise to trajectories that are more rectilinear. At a fixed tumble rate, optimal tumbling angles have been identified.

Finally, we presented a model where the reorientations are realized dynamically. The particles move intermittently,

and while in immobile phases with no translational motion, reorient according to Langevin dynamics with rotational diffusion coefficient D_S and chirality ω_S . Parameter space regions for which diffusion can be enhanced were discussed.

In the future, it would be interesting to explore further hybrid active dynamics, or even include more than two dynamical modes as presented here. It would also be of interest to see whether intermittent motion in three-dimensional helical motion could lead to similar enhancements of diffusivity [83–87]. For navigation problems where motion in a specific direction is desirable, such as in chemotaxis, it would be interesting to study the optimal reorientations that enhance the effective drift for chiral particles, not only effective diffusion [64,88,89]. Furthermore, many real-world examples of active matter reside in heterogeneous environments where optimal navigation past obstacles or other types of disorder is a crucial task [3,90–100]. Whether hybrid motility patterns can be beneficial in this case should also be explored.

ACKNOWLEDGMENTS

The authors acknowledge support from the Deutsche Forschungsgemeinschaft (DFG) within the project LO 418/29-1.

-
- [1] M. C. Marchetti, J.-F. Joanny, S. Ramaswamy, T. B. Liverpool, J. Prost, M. Rao, and R. A. Simha, Hydrodynamics of soft active matter, *Rev. Mod. Phys.* **85**, 1143 (2013).
 - [2] J. Elgeti, R. G. Winkler, and G. Gompper, Physics of microswimmers—Single particle motion and collective behavior: A review, *Rep. Prog. Phys.* **78**, 056601 (2015).
 - [3] C. Bechinger, R. Di Leonardo, H. Löwen, C. Reichhardt, G. Volpe, and G. Volpe, Active particles in complex and crowded environments, *Rev. Mod. Phys.* **88**, 045006 (2016).
 - [4] J. O’Byrne, Y. Kafri, J. Tailleur, and F. van Wijland, Time irreversibility in active matter, from micro to macro, *Nat. Rev. Phys.* **4**, 167 (2022).
 - [5] É. Fodor, R. L. Jack, and M. E. Cates, Irreversibility and biased ensembles in active matter: Insights from stochastic thermodynamics, *Annu. Rev. Condens. Matter Phys.* **13**, 215 (2022).
 - [6] S. van Teeffelen and H. Löwen, Dynamics of a Brownian circle swimmer, *Phys. Rev. E* **78**, 020101(R) (2008).
 - [7] H. Löwen, Chirality in microswimmer motion: From circle swimmers to active turbulence, *Eur. Phys. J.: Spec. Top.* **225**, 2319 (2016).
 - [8] P. D. Frymier, R. M. Ford, H. C. Berg, and P. T. Cummings, Three-dimensional tracking of motile bacteria near a solid planar surface, *Proc. Natl. Acad. Sci.* **92**, 6195 (1995).
 - [9] W. R. DiLuzio, L. Turner, M. Mayer, P. Garstecki, D. B. Weibel, H. C. Berg, and G. M. Whitesides, *Escherichia coli* swim on the right-hand side, *Nature (London)* **435**, 1271 (2005).
 - [10] E. Lauga, W. R. DiLuzio, G. M. Whitesides, and H. A. Stone, Swimming in circles: Motion of bacteria near solid boundaries, *Biophys. J.* **90**, 400 (2006).
 - [11] J. Hu, A. Wysocki, R. G. Winkler, and G. Gompper, Physical sensing of surface properties by microswimmers—Directing bacterial motion via wall slip, *Sci. Rep.* **5**, 9586 (2015).
 - [12] S. Bianchi, F. Saglimbeni, and R. Di Leonardo, Holographic imaging reveals the mechanism of wall entrapment in swimming bacteria, *Phys. Rev. X* **7**, 011010 (2017).
 - [13] F. Kümmel, B. ten Hagen, R. Wittkowski, I. Buttinoni, R. Eichhorn, G. Volpe, H. Löwen, and C. Bechinger, Circular motion of asymmetric self-propelling particles, *Phys. Rev. Lett.* **110**, 198302 (2013).
 - [14] B. Zhang, A. Sokolov, and A. Snezhko, Reconfigurable emergent patterns in active chiral fluids, *Nat. Commun.* **11**, 4401 (2020).
 - [15] M. Workamp, G. Ramirez, K. E. Daniels, and J. A. Dijkstra, Symmetry-reversals in chiral active matter, *Soft Matter* **14**, 5572 (2018).
 - [16] C. Scholz, A. Ldov, T. Pöschel, M. Engel, and H. Löwen, Surfactants and rotelles in active chiral fluids, *Sci. Adv.* **7**, eabf8998 (2021).
 - [17] F. J. Sevilla, Diffusion of active chiral particles, *Phys. Rev. E* **94**, 062120 (2016).
 - [18] L. Caprini and U. M. B. Marconi, Active particles under confinement and effective force generation among surfaces, *Soft Matter* **14**, 9044 (2018).

- [19] L. Caprini and U. M. B. Marconi, Active chiral particles under confinement: Surface currents and bulk accumulation phenomena, *Soft Matter* **15**, 2627 (2019).
- [20] L. Caprini, H. Löwen, and U. M. B. Marconi, Chiral active matter in external potentials, *Soft Matter* **19**, 6234 (2023).
- [21] B. Liebchen and D. Levis, Collective behavior of chiral active matter: Pattern formation and enhanced flocking, *Phys. Rev. Lett.* **119**, 058002 (2017).
- [22] V. E. Debets, H. Löwen, and L. M. C. Janssen, Glassy dynamics in chiral fluids, *Phys. Rev. Lett.* **130**, 058201 (2023).
- [23] E. Perez Ipiña, S. Otte, R. Pontier-Bres, D. Czerucka, and F. Peruani, Bacteria display optimal transport near surfaces, *Nat. Phys.* **15**, 610 (2019).
- [24] K. S. Olsen, Diffusion of active particles with angular velocity reversal, *Phys. Rev. E* **103**, 052608 (2021).
- [25] C. Weber, P. K. Radtke, L. Schimansky-Geier, and P. Hänggi, Active motion assisted by correlated stochastic torques, *Phys. Rev. E* **84**, 011132 (2011).
- [26] P. Bayati and A. Nourhani, Memory effects in spiral diffusion of rotary self-propellers, *Phys. Rev. E* **105**, 024606 (2022).
- [27] T. A. Witten and H. Diamant, A review of shaped colloidal particles in fluids: Anisotropy and chirality, *Rep. Prog. Phys.* **83**, 116601 (2020).
- [28] H. C. Berg and L. Turner, Chemotaxis of bacteria in glass capillary arrays. *Escherichia coli*, motility, microchannel plate, and light scattering, *Biophys. J.* **58**, 919 (1990).
- [29] A. Van Leeuwenhoek, Observations, communicated to the publisher by Mr. Antony van Leewenhoek, in a Dutch letter of the 9th octob. 1676. here English'd: Concerning little animals by him observed in rain-well-sea-and snow water; as also in water wherein pepper had lain infused, *Philos. Trans. R. Soc. London* **12**, 821 (1677).
- [30] G. I. Taylor, Diffusion by continuous movements, *Proc. London Math. Soc.* **s2-20**, 196 (1922).
- [31] S. Goldstein, On diffusion by discontinuous movements, and on the telegraph equation, *Q. J. Mech. Appl. Math.* **4**, 129 (1951).
- [32] H. Gupta, Diffusion by discrete movements, *Sankhyā: Indian J. Stat.* **20**, 295 (1958).
- [33] M. Kac, A stochastic model related to the telegrapher's equation, *Rocky Mt. J. Math.* **4**, 497 (1974).
- [34] H. C. Berg and D. A. Brown, Chemotaxis in *Escherichia coli* analysed by three-dimensional tracking, *Nature (London)* **239**, 500 (1972).
- [35] P. S. Lovely and F. Dahlquist, Statistical measures of bacterial motility and chemotaxis, *J. Theor. Biol.* **50**, 477 (1975).
- [36] M. J. Schnitzer, Theory of continuum random walks and application to chemotaxis, *Phys. Rev. E* **48**, 2553 (1993).
- [37] H. G. Othmer and T. Hillen, The diffusion limit of transport equations derived from velocity-jump processes, *SIAM J. Appl. Math.* **61**, 751 (2000).
- [38] H. G. Othmer and T. Hillen, The diffusion limit of transport equations II: Chemotaxis equations, *SIAM J. Appl. Math.* **62**, 1222 (2002).
- [39] R. Erban and H. G. Othmer, From individual to collective behavior in bacterial chemotaxis, *SIAM J. Appl. Math.* **65**, 361 (2004).
- [40] J. Tailleur and M. E. Cates, Statistical mechanics of interacting run-and-tumble bacteria, *Phys. Rev. Lett.* **100**, 218103 (2008).
- [41] M. Polin, I. Tuval, K. Drescher, J. P. Gollub, and R. E. Goldstein, *Chlamydomonas* swims with two “gears” in a eukaryotic version of run-and-tumble locomotion, *Science* **325**, 487 (2009).
- [42] F. Thiel, L. Schimansky-Geier, and I. M. Sokolov, Anomalous diffusion in run-and-tumble motion, *Phys. Rev. E* **86**, 021117 (2012).
- [43] K. Malakar, V. Jemseena, A. Kundu, K. V. Kumar, S. Sabhapandit, S. N. Majumdar, S. Redner, and A. Dhar, Steady state, relaxation and first-passage properties of a run-and-tumble particle in one-dimension, *J. Stat. Mech.: Theory Exp.* (2018) 043215.
- [44] A. Villa-Torrealba, C. Chávez-Raby, P. de Castro, and R. Soto, Run-and-tumble bacteria slowly approaching the diffusive regime, *Phys. Rev. E* **101**, 062607 (2020).
- [45] F. Mori, P. Le Doussal, S. N. Majumdar, and G. Schehr, Universal properties of a run-and-tumble particle in arbitrary dimension, *Phys. Rev. E* **102**, 042133 (2020).
- [46] D. Frydel, The run-and-tumble particle model with four-states: Exact solution at zero temperature, *Phys. Fluids* **34**, 027111 (2022).
- [47] I. Santra, U. Basu, and S. Sabhapandit, Run-and-tumble particles in two dimensions under stochastic resetting conditions, *J. Stat. Mech.: Theory Exp.* (2020) 113206.
- [48] D. Breoni, F. J. Schwarzendahl, R. Blossey, and H. Löwen, A one-dimensional three-state run-and-tumble model with a ‘cell cycle’, *Eur. Phys. J. E* **45**, 83 (2022).
- [49] B. Loewe, T. Kozhukhov, and T. N. Shendruk, Anisotropic run-and-tumble-turn dynamics, *Soft Matter* **20**, 1133 (2024).
- [50] M. R. Bailey, A. R. Sprenger, F. Grillo, H. Löwen, and L. Isa, Fitting an active Brownian particle's mean-squared displacement with improved parameter estimation, *Phys. Rev. E* **106**, L052602 (2022).
- [51] J. Taktikos, H. Stark, and V. Zaburdaev, How the motility pattern of bacteria affects their dispersal and chemotaxis, *PLoS ONE* **8**, e81936 (2013).
- [52] K. S. Olsen and H. Löwen, Dynamics of inertial particles under velocity resetting, *J. Stat. Mech.: Theory Exp.* (2024) 033210.
- [53] Y. Wu, A. D. Kaiser, Y. Jiang, and M. S. Alber, Periodic reversal of direction allows Myxobacteria to swarm, *Proc. Natl. Acad. Sci. USA* **106**, 1222 (2009).
- [54] S. Thutupalli, M. Sun, F. Bunyak, K. Palaniappan, and J. W. Shaevitz, Directional reversals enable *Myxococcus xanthus* cells to produce collective one-dimensional streams during fruiting-body formation, *J. R. Soc. Interface* **12**, 20150049 (2015).
- [55] S. Leonardy, I. Bulyha, and L. Søgaard-Andersen, Reversing cells and oscillating motility proteins, *Mol. Biosyst.* **4**, 1009 (2008).
- [56] B. L. Taylor and D. Koshland, Jr., Reversal of flagellar rotation in monotrichous and peritrichous bacteria: Generation of changes in direction, *J. Bacteriol.* **119**, 640 (1974).
- [57] J. E. Johansen, J. Pinhassi, N. Blackburn, U. L. Zweifel, and Å. Hagström, Variability in motility characteristics among marine bacteria, *Aquatic Microbial Ecology* **28**, 229 (2002).
- [58] J. I. Quelas, M. J. Althabegoiti, C. Jimenez-Sanchez, A. A. Melgarejo, V. I. Marconi, E. J. Mongiardini, S. A. Trejo, F. Mengucci, J.-J. Ortega-Calvo, and A. R. Lodeiro, Swimming

- performance of *Bradyrhizobium diazoefficiens* is an emergent property of its two flagellar systems, *Sci. Rep.* **6**, 23841 (2016).
- [59] R. Großmann, F. Peruani, and M. Bär, Diffusion properties of active particles with directional reversal, *New J. Phys.* **18**, 043009 (2016).
- [60] I. Santra, U. Basu, and S. Sabhapandit, Active Brownian motion with directional reversals, *Phys. Rev. E* **104**, L012601 (2021).
- [61] I. Santra, U. Basu, and S. Sabhapandit, Direction reversing active Brownian particle in a harmonic potential, *Soft Matter* **17**, 10108 (2021).
- [62] K. S. Olsen, L. Angheluta, and E. G. Flekkøy, Collective states of active matter with stochastic reversals: Emergent chiral states and spontaneous current switching, *Phys. Rev. Res.* **4**, 043017 (2022).
- [63] J. G. Mitchell, The energetics and scaling of search strategies in bacteria, *Am. Nat.* **160**, 727 (2002).
- [64] F. Mori and L. Mahadevan, Optimal switching strategies for navigation in stochastic settings, [arXiv:2311.18813](https://arxiv.org/abs/2311.18813).
- [65] R. Mallikarjun and A. Pal, Chiral run-and-tumble walker: Transport and optimizing search, *Physica A* **622**, 128821 (2023).
- [66] H. Larralde, Transport properties of a two-dimensional “chiral” persistent random walk, *Phys. Rev. E* **56**, 5004 (1997).
- [67] K. Singwi and A. Sjölander, Diffusive motions in water and cold neutron scattering, *Phys. Rev.* **119**, 863 (1960).
- [68] G. H. Weiss, The diffusion constant for two-state Brownons, *J. Stat. Phys.* **8**, 221 (1973).
- [69] A. Datta, C. Beta, and R. Großmann, The random walk of intermittently self-propelled particles, [arXiv:2406.15277](https://arxiv.org/abs/2406.15277).
- [70] I. Santra, K. S. Olsen, and D. Gupta, Dynamics of switching processes: general results and applications in intermittent active motion, *Soft Matter* **20**, 9360 (2024).
- [71] T. J. Doerries, A. V. Chechkin, R. Schumer, and R. Metzler, Rate equations, spatial moments, and concentration profiles for mobile-immobile models with power-law and mixed waiting time distributions, *Phys. Rev. E* **105**, 014105 (2022).
- [72] T. J. Doerries, A. V. Chechkin, and R. Metzler, Apparent anomalous diffusion and non-Gaussian distributions in a simple mobile-immobile transport model with Poissonian switching, *J. R. Soc. Interface* **19**, 20220233 (2022).
- [73] T. J. Doerries, R. Metzler, and A. V. Chechkin, Emergent anomalous transport and non-gaussianity in a simple mobile-immobile model: The role of advection, *New J. Phys.* **25**, 063009 (2023).
- [74] F. Peruani and D. Chaudhuri, Active stop and go motion: A strategy to improve spatial exploration?, [arXiv:2306.05647](https://arxiv.org/abs/2306.05647).
- [75] J. Saragosti, P. Silberzan, and A. Buguin, Modeling *E. coli* tumbles by rotational diffusion. implications for chemotaxis, *PLoS ONE* **7**, e35412 (2012).
- [76] F. Detcheverry, Generalized run-and-turn motions: From bacteria to Lévy walks, *Phys. Rev. E* **96**, 012415 (2017).
- [77] F. Mori, P. Le Doussal, S. N. Majumdar, and G. Schehr, Condensation transition in the late-time position of a run-and-tumble particle, *Phys. Rev. E* **103**, 062134 (2021).
- [78] A. K. Hartmann, S. N. Majumdar, H. Schawe, and G. Schehr, The convex hull of the run-and-tumble particle in a plane, *J. Stat. Mech.: Theory Exp.* (2020) 053401.
- [79] P. Singh, A. Kundu, S. N. Majumdar, and H. Schawe, Mean area of the convex hull of a run and tumble particle in two dimensions, *J. Phys. A: Math. Theor.* **55**, 225001 (2022).
- [80] K. S. Olsen, D. Gupta, F. Mori, and S. Krishnamurthy, Thermodynamic cost of finite-time stochastic resetting, *Phys. Rev. Res.* **6**, 033343 (2024).
- [81] F. Mori, K. S. Olsen, and S. Krishnamurthy, Entropy production of resetting processes, *Phys. Rev. Res.* **5**, 023103 (2023).
- [82] K. S. Olsen and D. Gupta, Thermodynamic work of partial resetting, *J. Phys. A: Math. Theor.* **57**, 245001 (2024).
- [83] H. S. Jennings, On the significance of the spiral swimming of organisms, *Am. Nat.* **35**, 369 (1901).
- [84] B. M. Friedrich and F. Jülicher, Chemotaxis of sperm cells, *Proc. Natl. Acad. Sci. USA* **104**, 13256 (2007).
- [85] R. Wittkowski and H. Löwen, Self-propelled Brownian spinning top: Dynamics of a biaxial swimmer at low reynolds numbers, *Phys. Rev. E* **85**, 021406 (2012).
- [86] R. E. Goldstein, Green algae as model organisms for biological fluid dynamics, *Annu. Rev. Fluid Mech.* **47**, 343 (2015).
- [87] J. B. Kirkegaard, A. O. Marron, and R. E. Goldstein, Motility of colonial choanoflagellates and the statistics of aggregate random walkers, *Phys. Rev. Lett.* **116**, 038102 (2016).
- [88] K. C. Leptos, M. Chioccioli, S. Furlan, A. I. Pesci, and R. E. Goldstein, Phototaxis of *Chlamydomonas* arises from a tuned adaptive photoresponse shared with multicellular Volvocine green algae, *Phys. Rev. E* **107**, 014404 (2023).
- [89] Y. Baouche, T. Franosch, M. Meiners, and C. Kurzthaler, Active Brownian particle under stochastic orientational resetting, [arXiv:2405.06769](https://arxiv.org/abs/2405.06769).
- [90] T. Bertrand, Y. Zhao, O. Bénichou, J. Tailleur, and R. Voituriez, Optimized diffusion of run-and-tumble particles in crowded environments, *Phys. Rev. Lett.* **120**, 198103 (2018).
- [91] S. Makarchuk, V. C. Braz, N. A. M. Araújo, L. Ciric, and G. Volpe, Enhanced propagation of motile bacteria on surfaces due to forward scattering, *Nat. Commun.* **10**, 4110 (2019).
- [92] R. Alonso-Matilla, B. Chakrabarti, and D. Saintillan, Transport and dispersion of active particles in periodic porous media, *Phys. Rev. Fluids* **4**, 043101 (2019).
- [93] O. Chepizhko and T. Franosch, Random motion of a circle microswimmer in a random environment, *New J. Phys.* **22**, 073022 (2020).
- [94] K. S. Olsen, L. Angheluta, and E. G. Flekkøy, Active Brownian particles moving through disordered landscapes, *Soft Matter* **17**, 2151 (2021).
- [95] C. Kurzthaler, S. Mandal, T. Bhattacharjee, H. Löwen, S. S. Datta, and H. A. Stone, A geometric criterion for the optimal spreading of active polymers in porous media, *Nat. Commun.* **12**, 7088 (2021).
- [96] D. M. van Roon, G. Volpe, M. M. T. da Gama, and N. A. M. Araújo, The role of disorder in the motion of chiral active particles in the presence of obstacles, *Soft Matter* **18**, 6899 (2022).

- [97] D. Saintillan, Dispersion of run-and-tumble microswimmers through disordered media, *Phys. Rev. E* **108**, 064608 (2023).
- [98] C. Lohrmann and C. Holm, Optimal motility strategies for self-propelled agents to explore porous media, *Phys. Rev. E* **108**, 054401 (2023).
- [99] K. S. Olsen, A. Hansen, and E. G. Flekkøy, Hyper-ballistic superdiffusion of competing microswimmers, *Entropy* **26**, 274 (2024).
- [100] C. Jin and A. Sengupta, Microbes in porous environments: From active interactions to emergent feedback, *Biophys. Rev.* **16**, 173 (2024).